

Corrosion Behavior of Carbon Steel with Pearlite-Ferrite Microstructure in Water-Saturated Supercritical H₂S/CO₂ Environment

Chi Yu^{1,2,*}, Hongwei Wang³, Xiuhua Gao⁴

¹ School of Resources and Materials, Northeastern University at Qinhuangdao, Qinhuangdao 066004, China;

² School of Mechanical Engineering, Yanshan University, Qinhuangdao 066000, China;

³ School of Control Engineering, Northeastern University at Qinhuangdao, Qinhuangdao 066004, China;

⁴ The State Key Laboratory of Rolling and Automation, Northeastern University, Shenyang 110819, China

*E-mail: yuchi0319@163.com

Received: 23 March 2017 / Accepted: 30 December 2017 / Published: 10 May 2018

The corrosion characteristics of carbon steel with pearlite-ferrite microstructure in water-saturated supercritical H₂S/CO₂ environment are analyzed. The whole corrosion process is divided into three stages, the grain shape and morphology of corrosion products are studied by scanning electron microscopy (SEM) and X-ray diffraction (XRD). The results show Fe-S compounds change from iron-rich mackinawite to sulfur-rich pyrrhotite with increasing immersion time, and troilite as intermediate product during the transformation sequence. The corrosion rate decreases rapidly when pyrrhotite forms, it could effectively protect the steel substrate to inhibit corrosion.

Keywords: carbon steel, H₂S/CO₂ environment, corrosion characteristics, SEM, XRD

1. INTRODUCTION

With the fast development of oil and gas industry, the corrosion problem of carbon steel has attracted more attention because of the special work conditions with considerable amount of H₂S and CO₂, which will lead to catastrophic accident and huge economic loss [1-4]. At present, the application of carbon steels is more popular for tubings since carbon steel are more cost-effective and excellent mechanical properties, so it is essential to study the corrosion characteristics.

The corrosion behavior of carbon steel under H₂S and CO₂ environment is firstly studied in the 1940s, and some results have been obtained [5-8]. Masamura et al have investigated a critical ratio of P_{H_2S}/P_{CO_2} to understand the corrosion mechanism of carbon steel. They have found when $P_{H_2S}/P_{CO_2} < 200$, the corrosion products are FeS and FeCO₃, when $P_{H_2S}/P_{CO_2} > 200$, the corrosion products are mainly FeCO₃, it indicates that CO₂ plays an important role during the corrosion process [9]. Pots et al have presented that when $P_{H_2S}/P_{CO_2} > 500$, CO₂ plays a significant role, when $P_{H_2S}/P_{CO_2} < 20$, H₂S has a major influence on the whole reaction process, and when $20 < P_{H_2S}/P_{CO_2} < 500$, the corrosion behaviors are controlled by H₂S and CO₂ simultaneously [10]. Li et al. have researched the corrosion properties of tubing steel in environment with high H₂S and CO₂ content and the results show that the H₂S has an important influence and precipitation of iron sulfide on the steel surface is superior to iron carbonate [5]. Wei et al have investigated the effect of small amount of H₂S on the corrosion behavior of carbon steel in the CO₂ environment, and analyze the composition of corrosion products [11]. Zhao et al. have studied that the corrosion behavior about Ni-based alloys in simulation solution containing H₂S/CO₂ at different temperature [12]. They have investigated the effects of alloy element Cr on corrosion resistance in CO₂/H₂S environment, respectively [13-14]. Wang et al have proposed that the corrosion behaviors of Ni-Cr-Mo laser coating, stainless steel and X70 steel in different simulated solutions with H₂S/CO₂ [15]. The effect of H₂S impurity on the corrosion behavior of X65 steel in CO₂ system is also investigated, and they have proposed the H₂S corrosion risk cannot be ignored [16-17]. Some results about the H₂S and CO₂ corrosion are also obtained by electrochemical method [12,18-23]. It is worth noting that many researchers have studied the effect of some conditions including temperature, pH value, microstructure, gas content and alloying elements on the corrosion resistant performance. Corrosion is a complex process, and the corrosion mechanism changes as the immersion time increases. It is known that various corrosion products have different effects on carbon steel in H₂S/CO₂ environments due to their physico-chemical characteristics. The works about H₂S/CO₂ corrosion are few because of the highly toxic and corrosion nature, the corrosion behavior will become very complex when the water in oil and gas encounters H₂S and CO₂. Some published papers have studied the initial stage of corrosion behavior [24-26]. But its detailed mechanism for long period is not yet studied completely, especially the corrosion property of pearlite-ferrite steel under H₂S/CO₂ coexistence environments is still poorly understand.

The aim of this work is to investigate the effect varying corrosion products on the corrosion behavior of pearlite-ferrite steel by immersion experiment and electrochemical method in water-saturated supercritical H₂S and CO₂ environments, the total pressure is 1.2 MPa ($P_{CO_2}/P_{H_2S}=7$), the experimental temperature is 75°C. The corrosion rate is obtained through the mass loss method. And the polarization curve and electrochemical impedance spectroscopy (EIS) are given to analyze electrochemical corrosion behavior, and using tafel fitting and equivalent circuit method, respectively. The surface morphology and structure of corrosion products are investigated by scanning electron microscope (SEM) and X-ray diffraction (XRD). These results are of great value for H₂S and CO₂ corrosion mitigation. It can provide the basic theoretical reference to develop pearlite-ferrite steel for oil and gas industry.

2. EXPERIMENTAL

2.1 Specimen preparation

The carbon steel composed of following elements (wt.%) of 0.15 C, 0.30 Si, 1.36 Mn, 0.013 P, 0.009 S, 0.030Al, 0.06 Nb, 0.03Ti and Fe (balance) is used in this study. The amount of carbon element is controlled slightly high, the amounts of P and S are limited to 0.013% and 0.009% to reduce the pollution, respectively, the Nb and Ti elements as main microalloyed elements are added in it. The raw materials are smelted, forged and thermo-mechanical control process including final rolling temperature for 847°C, final cooling temperature for 652°C and cooling rate for 10.7°C/s. The specimens for immersion test are cut into 20 mm × 25 mm × 4 mm with a 3 mm diameter hole on the edge. The electrochemical samples are cut into 10 mm × 10 mm × 3 mm, and only a surface with 10 mm×10 mm is exposed to the solution, other surfaces are isolated by epoxy resin. Prior to testing, all the specimens are ground with silicon carbide paper from 600 to 1500 grit, rinsed with ethanol and degreased with acetone, and then dried with cold air. The samples are weighted using a balance with a precision of 0.01mg and stored in a desiccator.

2.2 Experimental methods

All samples are placed in a high temperature and high pressure autoclave with 5 L capacity. The test electrolyte with volume of 4 L is 3.5 wt% NaCl, which is prepared from distilled water and an analytical reagent. First, the electrolyte solution is injected in the autoclave. N₂ is bubbled into the test solution for 3 h to deoxygenate and the tested samples are immersed in the solution and sealed autoclave. Second, N₂ is purged into the test electrolyte again to deoxygenate for 0.5 h. The electrolyte is heated to 75 °C using the circulatory oil system. Third, the mixed gas is continuously poured in the electrolyte solution until the pressure reached to 1.2MPa with partial pressure 0.09 MPa H₂S, 0.64 MPa CO₂ and 0.47 MPa N₂, the gas purity used in the experiment is 99.99%. The experimental pressure is obtained by assuming that the H₂S/CO₂ gas permeated continuously in the armour layer for a designed longevity of 20 years. Four immersion time of 48 h, 96 h, 192 h and 384 h are chosen to study the corrosion mechanism. The specimens used to calculate the mass loss are removed from high pressure autoclave, and rinsed with deionized water. The chemical cleaning method is used to remove the corrosion scale. The chemical method with the etching solution compositions of 50 ml 37% HCl, 5g hexamethy lenetebamine (urotropine) and 450 ml deionized water is chosen to descale the scale, dried in the air and finally weighted. Three parallel samples are used to perform each immersion test to ensure reproducibility, and the average mass loss is obtained. The corrosion rate is calculated by the following equation.

$$v = \frac{8.76 \times 10^4 \times \Delta W}{S \times T \times \rho} \quad (1)$$

where v is the average corrosion rate (mm/year), ΔW is the mass loss(g), S is the total surface of the samples (cm²), T is the corrosion time (h), ρ is the physical density of the carbon steel (7.86 g/cm³).

The electrochemical experiments are performed with PATSTAT2273 workstation. A conventional three-electrode cell is used for the polarization curve and electrochemical impedance spectroscopy tests. A platinum electrode is used as the auxiliary electrode, a saturated calomel electrode (SCE) is used as the reference electrode, and the carbon steel is used as the working electrode. All polarization curves are obtained with scan rate of 0.1 mV/s. The EIS experiments are carried out at open circuit voltage using alternating current voltage amplitude of 8 mV and a frequency range is from 100 kHz to 0.1 Hz. The mixed gas is continuously poured in the aerated 3.5 wt% NaCl solution with partial pressure 0.09 MPa H₂S, 0.64 MPa CO₂ and 0.47 MPa N₂, the electrolyte is kept at 75 °C.

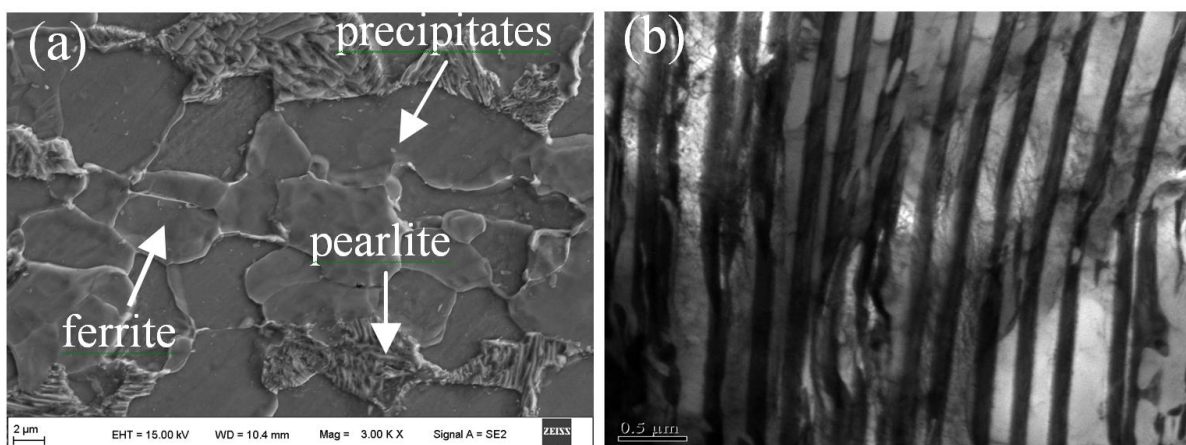
2.3 Morphology observation

The microstructures of carbon steel are observed by FEI QUANTA 600 scanning electron microscopy (SEM). The high-resolution FEI Tecnai G²F20 transmission electron microscope (TEM) is used to reveal the microstructure in detail. The surface morphology of corrosion products is examined by ZEISS ULTRA55 field emission scanning electron microscope equipped with EDX. The corrosion phases are detected using X-ray diffraction (XRD) with Co K α radiation and a step 0.04°. The crystal structure of corrosion products is identified by matching peak positions with MDI Jade software equipped with database PDF-2(2004).

3. RESULTS AND DISCUSSION

3.1 Microstructures

Many results have shown that the H₂S/CO₂ corrosion behaviour of carbon steel depends on its microstructure. So it is necessary to study the microstructure in this work. The microstructures characteristics are demonstrated in Fig.1. As seen, the microstructure is pearlite and ferrite. It indicates pro-eutectoid ferrite occupying mainly in grain boundary region, while prior-austenite grains have transformed into pearlite, the typical lamellar pearlite is observed by transmission electron microscope (TEM).



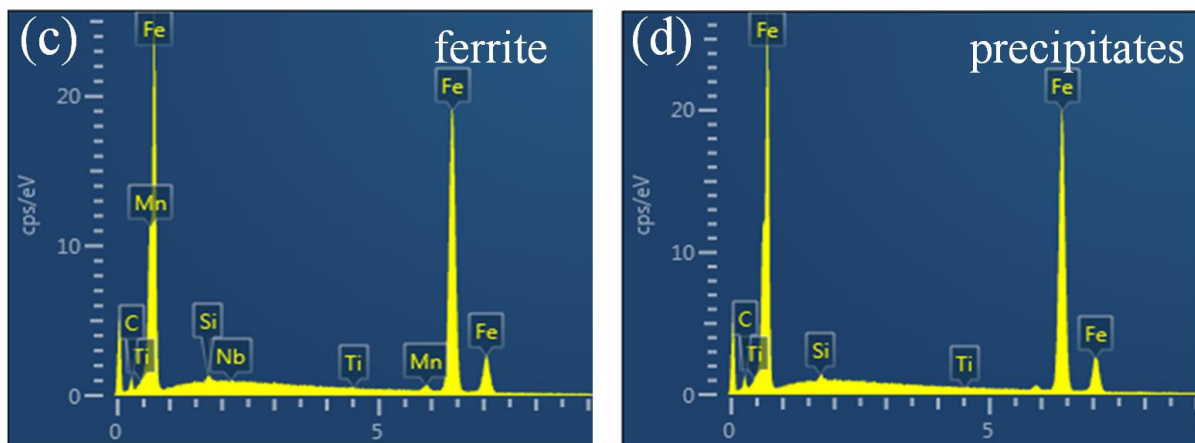


Figure 1. Microstructure characterization of carbon steel showed by (a) SEM, (b) TEM, (c) and (d) EDX

The energy dispersive X-ray spectroscopy (EDX) results show that the precipitate particles are rich in titanium, indicating that these particles are Ti-rich carbides.

3.2 Corrosion morphology characterization

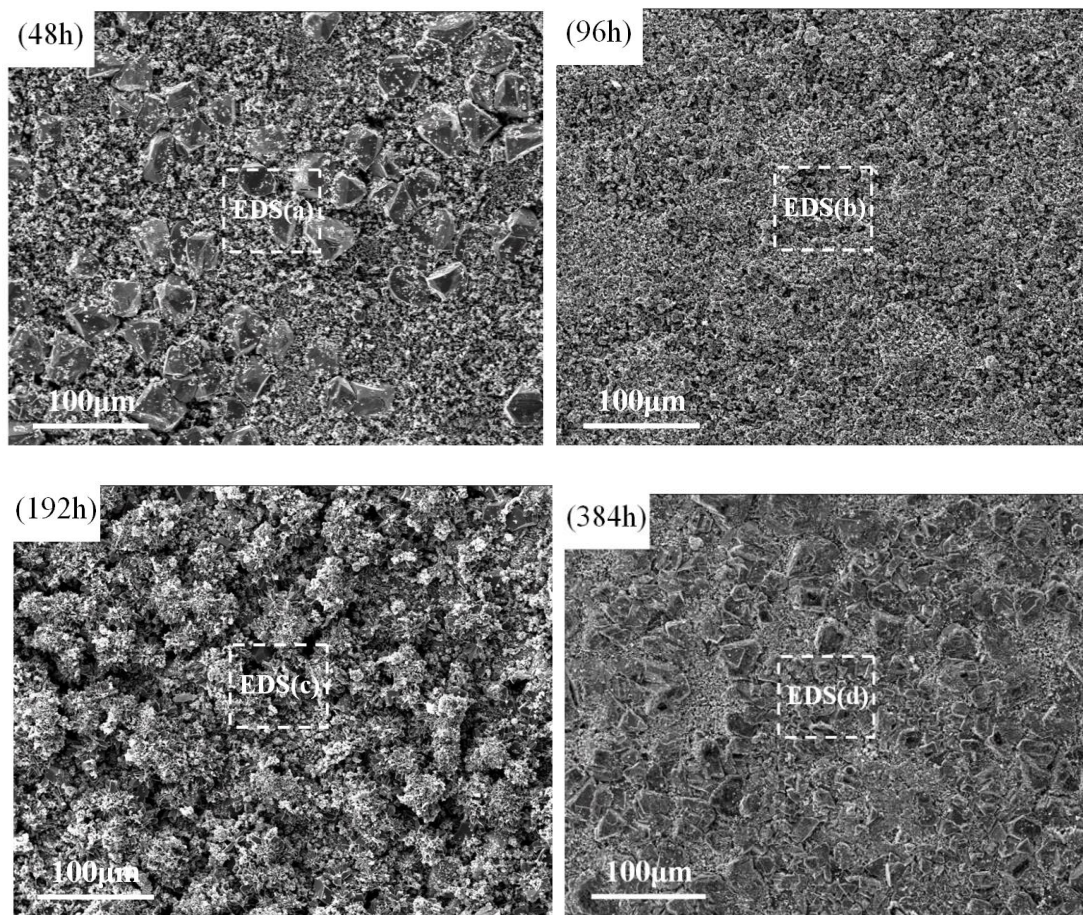
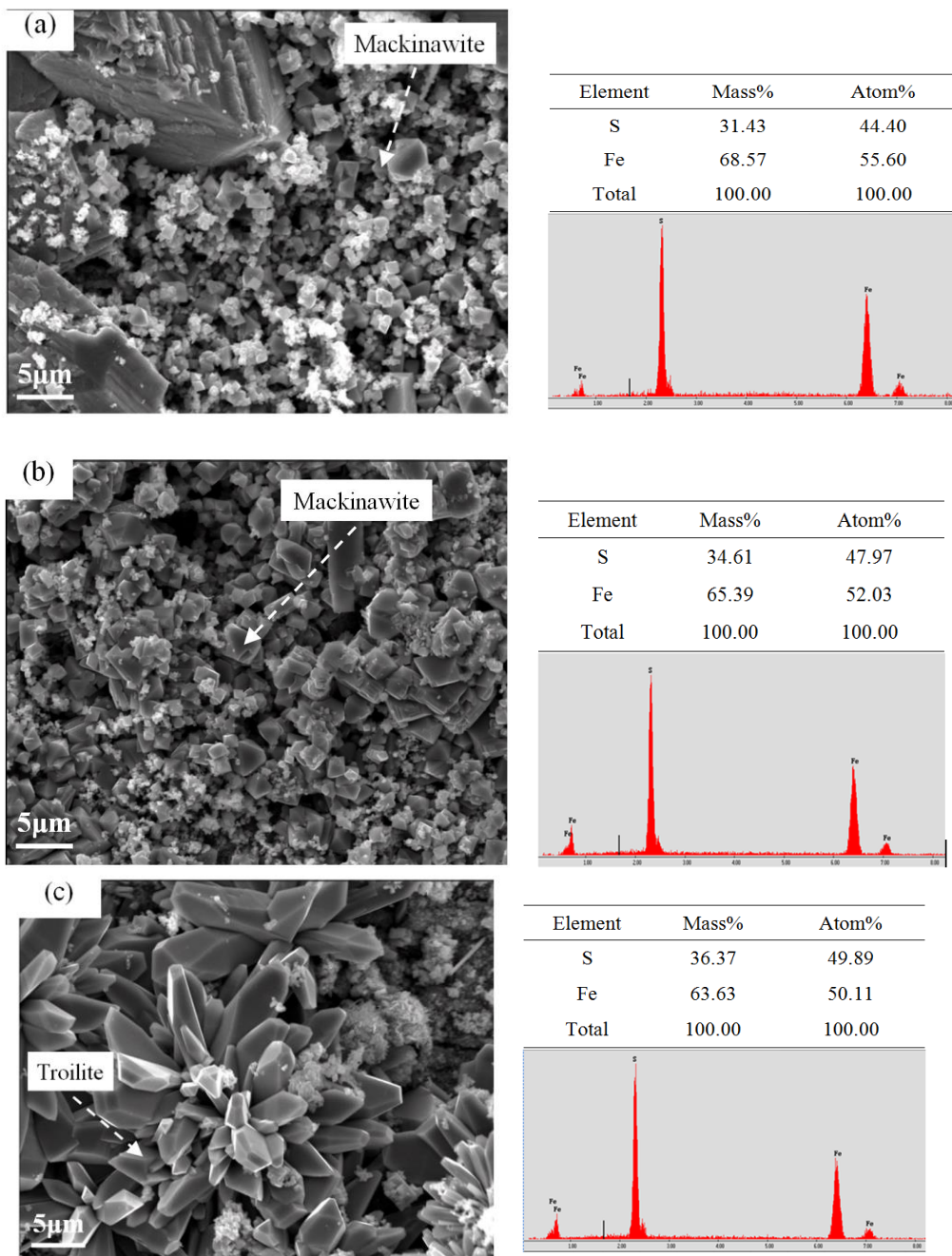


Figure 2. Surface corrosion morphology of carbon steel with pearlite-ferrite microstructure in H₂S and CO₂ environment at 75°C after different immersion time

Fig.2 and Fig.3 show the surface morphologies and EDX results of carbon steel immersed in sodium chloride solution containing H₂S and CO₂, respectively. After immersion 48 h, the corrosion products with mackinawite have formed on the steel surface. The corrosion particle is larger, arrangement between particles is not closer, the local position generates corrosion crack, and the phenomenon has a bad influence on the corrosion resistance. As the corrosion scales mainly composed of mackinawite grow thicker, it will crack and fall off as a result of stress due to the volume effect, therefore the corrosion product is very loose [27].



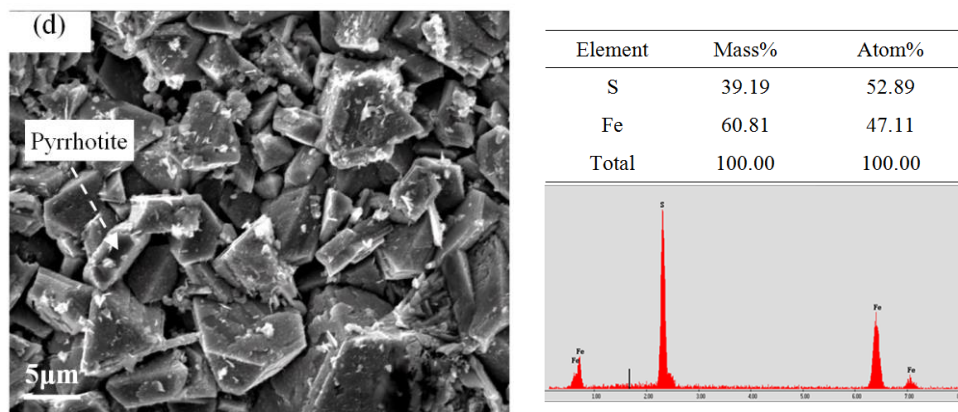
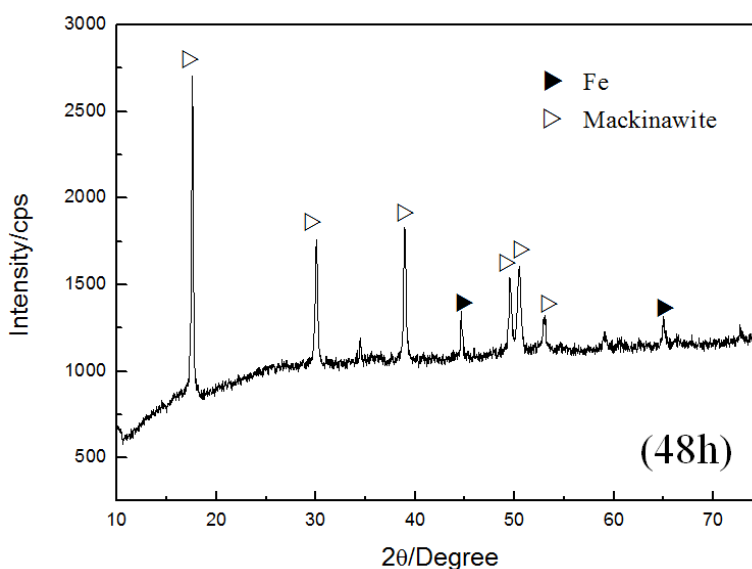


Figure 3. EDX results of carbon steel with pearlite-ferrite microstructure in H₂S and CO₂ environment at 75°C after different immersion time: (a)48h (b)96h (c)192h and (d)384h

It is seen that the large particle size may be fall off or dissolved when immersing 96 h, there is very compact corrosion products formed on the sample surface with the increasing concentration of S²⁻, the corrosion resistance is improved. Obviously, the protective ability of corrosion product films increases and corrosion rate decreases, so it can protect the steel matrix efficiently. Mackinawite is the initial corrosion product due to its rapid formation kinetics, then it transforms into other iron sulfides depending on environmental factors [28]. As immersion time increases, mackinawite is formed and dissolved, and the nucleation and growth of troilite and pyrrhotite occupy a main position. Troilite is the intermediate corrosion product, the pyrrhotite is feature of a hexagonal prism-like crystal, and the elongated hexagonal crystals seem to arise from troilite precursors, hexagonal prisms of pyrrhotite are thought to have nucleated independently of troilite [29]. With immersion time increases, the concentration of S²⁻ increases, and then forms sulfur-richer pyrrhotite.

3.3 Corrosion phases



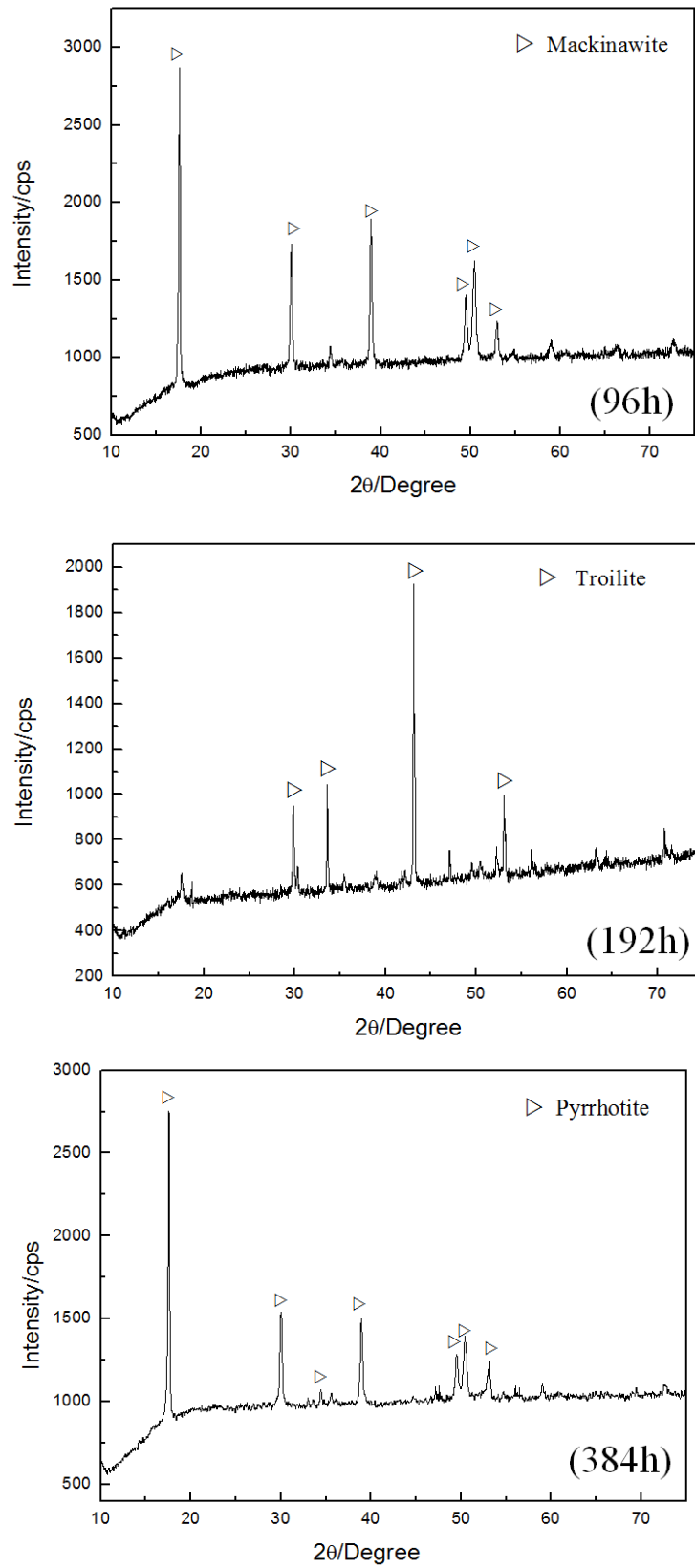


Figure 4. corrosion phases of carbon steel with pearlite-ferrite microstructure in H₂S and CO₂ environment at 75°C after different immersion time

The phase compositions of carbon steel after different immersion time are shown, the orientation of corrosion crystals is isotropic as different crystal faces are observed in Fig.4. The MDI Jade software is used to identify the styles of corrosion products based on the test data and theoretical analysis diffraction angles of different corrosion phases. It can be seen that the corrosion products are composed of different iron sulfide compounds, the absence of FeCO_3 in the corrosion scales indicates that the H_2S corrosion has a significant effect on the whole reaction process and iron sulfide is superior to precipitating on the steel surface compared with iron carbonate [26,30]. Only Fe is remained when immersed time 48h, the result may be attributed to the thin corrosion films are formed, mainly a few corrosion products appear at this time. When immersion time is 96 h, Fe is not detected. Then the corrosion product grows and adheres, the thickness of corrosion product films will increases. With immersion time increases, the mackinawite is formed and dissolved, and the nucleation and growth of troilite and pyrrhotite is gradually dominated. As a result, the main corrosion products vary from the iron-rich mackinawite to sulfur-rich troilite and pyrrhotite.

3.4 Mass loss method

Fig.5 shows the corrosion rate of carbon steel as a function of immersion time, the corrosion rate reveals basically the corrosion property of carbon steel.

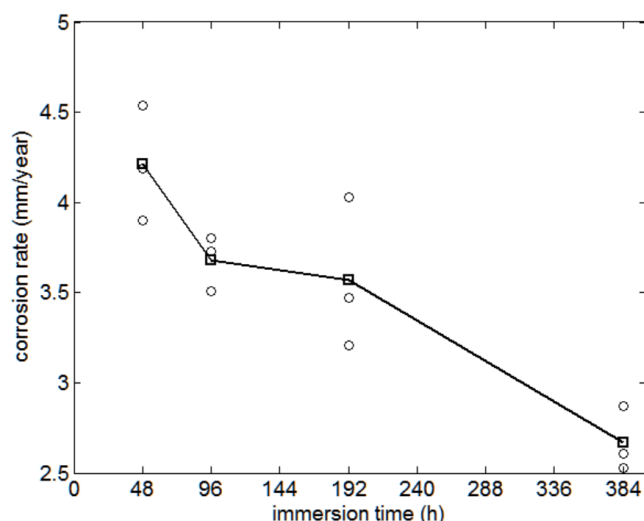


Figure 5. The corrosion rate curve of carbon steel with pearlite-ferrite microstructure in H_2S and CO_2 environment at 75°C after different immersion time (○: scatter value, □: average value)

It is seen that the corrosion rate decreases with increasing immersion time. The corrosion rate exhibits three distinguishable stages. It decreases quickly at the beginning, and changes slowly, then finally decreases. Mackinawite is the main corrosion product for immersion time 48 h and 96 h. And the corrosion rate decreases rapidly from 48 h to 96 h. This is maybe the more compact corrosion products are appeared. After that, the troilite is formed, and the corrosion rate changes slightly. Then the troilite transforms into pyrrhotite during the later stage, the corrosion rate decreases dramatically. It

is obvious that the pyrrhotite has protectiveness on carbon steel, and it can mitigate corrosion to some extent.

3.5 Potentiodynamic polarization curve measurement

The typical polarization curves of carbon steel in water-saturated supercritical H₂S/CO₂ environment after immersion time for 48 h, 96 h, 192 h and 384 h are shown in Fig.6. In this work, the purpose of the potentiodynamic polarization curve test is to study the effect of corrosion product. The corresponding anodic tafel constants (b_a), cathodic tafel constants (b_c), corrosion potential (E_{corr}) and corrosion current density (I_{corr}) obtained by extrapolation of tafel lines are shown in Table 1. The corrosion current density declines simultaneously with increasing immersion time from 48 h to 384 h. The carbon steel after immersion 384 h shows the well corrosion behavior with the smaller corrosion current density 0.07 mA.cm⁻², which indicate the corrosion product can effectively protect the steel substrate. Also, corrosion rate *v* is calculated based on the following equation [31].

$$v = 0.00327 \frac{ai}{nD} \tag{2}$$

where *a* is molar mass of steel (g/mol), *i* is corrosion current density (μA/cm²), *n* is valency, *D* is the physical density of carbon steel. It is found that the corrosion rate is proportional to corrosion current density. It is in coincidence with the results of weight loss analysis.

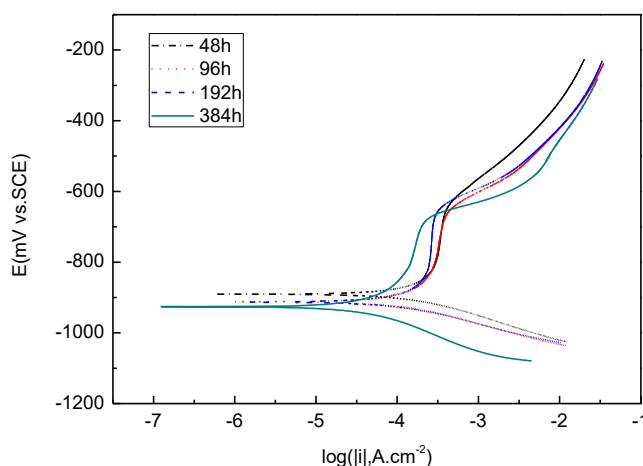


Figure 6. Potentiodynamic polarization curves of carbon steel with pearlite-ferrite microstructure in H₂S and CO₂ environment at 75°C after different immersion time

Table 1. Potentiodynamic polarization parameters from a curve-fitting approach

Immersion time/hour	b _a (mV/dec)	b _c (mV/dec)	E _{corr} (mV vs.SCE)	I _{corr} (mA.cm ⁻²)
48	927	-84	-891	0.25
96	481	-73	-912	0.17
192	552	-69	-913	0.16
384	329	-108	-926	0.07

3.6 EIS measurement

EIS can obtain some information on corrosion processes that occur on electrode surface. The typical Nyquist diagrams are shown in Fig.7. The curve includes an incomplete semicircle at low frequency, the diameters of semicircle for carbon steel after immersion 384 h is larger than others immersion time. After comparing some equivalent circuit diagrams, the diagram with the minimum error is chosen. The electrochemical equivalent circuit with two time constants is shown in Fig.8. Fitting results are given in Table 2. In the circuit, R_s represents the resistance of electrolyte solution. R_f represents the resistance of corrosion product film. R_{ct} represents the charge transfer resistance. CPE is the constant phase element representing the double-charge layer capacitance, which is expressed as follows.

$$Z_{CPE} = \frac{1}{Y_0(j\omega)^n} \tag{4}$$

where Y_0 is an admittance function, $j = (-1)^{1/2}$, $\omega = 2\pi f$ is the angular frequency, $n(0 < n < 1)$ is a power. CPE_f is total surface electrode capacitance after electrode surface dispersion, n_1 is dispersion effect index of CPE_f , For $n_1 = 1$, CPE_f is equivalent to the ideal capacitance, for $n_1 = 0$, CPE_f is equivalent to the ideal resistance. CPE_{dl} represents the capacitance for solution/metal surface in the corrosion hole, n_2 is dispersion effect index of CPE_{dl} [26]. The EIS fitting figures of carbon steel after different immersion time are shown in Fig.7.

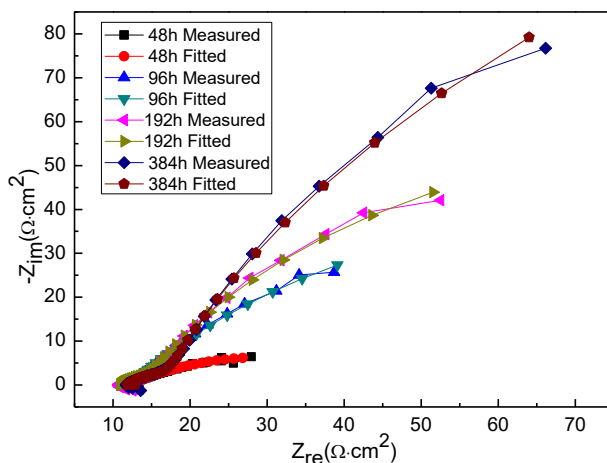


Figure 7. Nyquist plots of carbon steel with pearlite-ferrite microstructure in H₂S and CO₂ environment at 75°C after different immersion time

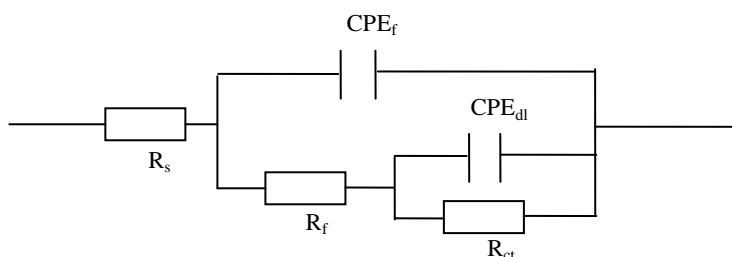


Figure 8. Equivalent circuit with two time constants

Table 2. EIS fitting results of carbon steel with pearlite-ferrite microstructure in H₂S and CO₂ environment at 75°C after different immersion time

Immersion time/hour	R _s (Ω·cm ²)	Y _f (S-sec ⁿ /cm ²)	n ₁	R _f (Ω·cm ²)	Y _{dl} (S-sec ⁿ /cm ²)	n ₂	R _{ct} (Ω·cm ²)
48	11.6	0.010	0.99	0.70	0.048	0.43	36
96	11.7	0.001	0.99	1.13	0.029	0.64	146
192	10.9	0.007	0.68	6.36	0.013	0.80	166
384	11.9	0.005	0.64	8.08	0.009	0.86	440

Based on the above analysis from Table 2, R_s is about 11.5 Ω·cm² and change a little, which show each test is in a stable state. With increasing immersion time, the resistances of corrosion product films (R_f) increase gradually, it reveals good corrosion resistance with the increase in film thickness. The R_{ct} values will increase from 36 Ω·cm² to 440 Ω·cm², the largest value is obtained for carbon steel after immersion 384 h, the smallest one is obtained for 48 h. The polarization resistance can be expressed as $R_p = R_{ct} + R_f$, which has been widely used to account for the kinetics of electrochemical corrosion, and the smaller the polarization resistance, the greater the corrosion rate [32]. This phenomenon suggests that Fe surface is uniformly covered with a corrosion product film. The uniform corrosion product films and dynamic corrosion product are protective in this experimental condition. The obtained result by the EIS is consistent with those obtained by weight loss and potentiodynamic polarization measurements.

4. CONCLUSIONS

The corrosion behavior of carbon steel with pearlite-ferrite microstructure has been investigated in sodium chloride solution containing H₂S and CO₂ for simulating the environment of oil and gas industry. Fe-S compounds with various shapes are formed during the corrosion process, it is divided into three stages, the corrosion rate decreases quickly at the beginning, and changes slowly, then finally decreases with increase immersion time. The corrosion products are changed in this sequence: mackinawite-troilite-pyrrhotite. Pyrrhotite with sulfur-rich FeS can effectively protect the steel substrate, and it will mitigate corrosion of carbon steel to some extent.

ACKNOWLEDGEMENTS

This work was supported by the Doctoral Scientific Research Foundation of Northeastern University at Qinhuangdao (No.XNB201717), the Technology Support Project of Northeastern University at Qinhuangdao (No.XNK201604), the Science and Technology Project of Hebei Province (No.15211028), the Natural Science Foundation of Liaoning Province (No.20170540310).

References

1. S. Nešić, *Corros. Sci.*, 49(2007)4308.

2. L. D. Paolinelli, T. Pérez and S. N. Simison, *Corros. Sci.*, 50(2008)2456.
3. B. Lemoine, Y. G. Li, R. Cadours, C. Bouallou and D. Richon, *Fluid Phase Equilib.*, 172(2000)261.
4. S. Zheng, C. Zhou, X. Chen, L. Zhang, J. Zheng and Y. Zhao, *Int. J. Hydrogen Energy*, 39(2014)13919.
5. W. F. Li, Y. J. Zhou and Y. Xue, *J. Iron Steel Res. Int.*, 19(2012)59.
6. W. He, O. Ø. Knudsen and S. Diplas, *Corros. Sci.*, 51(2009)2811.
7. Z. Aslam, R. A. Shawabkeh, I. A. Hussein, A. Al-baghli and M. Eic, *Appl. Surf. Sci.*, 327(2015)107.
8. H. S. Song, M. G. Park, E. Croiset, Z. W. Chen, S. C. Nam, H. J. Ryu and K. B. Yi, *Appl. Surf. Sci.*, 280(2013)360.
9. K. Masamura and S. Hashizume, *Corros.*, 43(1987)359.
10. B. F. M. Pot, S. D. Kapusta and R. C. John, *In: corrosion 2002, Houston*, 2002.
11. L. Wei, X. L. Pang and K. W. Gao, *Corros. Sci.*, 103(2016)132.
12. X. H. Zhao, Y. Han, Z. Q. Bai and B. Wei, *Electrochim. Acta*, 56(2011)7725.
13. L. D. Wang, H. B. Wu, Y. T. Liu, H. W. Zhang, L. F. Liu and D. Tang, *Mater. Sci. Technol.*, 21(2013)8.
14. H. B. Wu, L. F. Liu, L. D. Wang and Y. T. Liu, *J. Iron Steel Res. Int.*, 21(2014)76.
15. Q. Y. Wang, X. Z. Wang, H. Luo and J. L. Luo, *Surf. Coat. Tech.*, 291(2016)250.
16. C. Sun, Y. Wang, J. B. Sun, X. Q. Lin, X. D. Li, H. F. Liu and X. K. Cheng, *J. Supercrit. Fluid*, 116(2016)70.
17. J. B. Sun, C. Sun, G. A. Zhang, X. D. Li, W. M. Zhao, T. Jiang, H. F. Liu, X. K. Cheng and Y. Wang, *Corros. Sci.*, 107(2016)31.
18. G. A. Zhang, Y. Zeng and X. P. Guo, *Corros. Sci.*, 65(2012)37.
19. Z. F. Yin, W. Z. Zhao, Z. Q. Bai, Y. R. Feng and W. J. Zhou, *Electrochim. Acta*, 53(2008)3690.
20. X. H. Zhao, Y. Han, Z. Q. Bai and B. Wei, *Electrochim. Acta*, 56(2011)7725.
21. C. Yu, P. Wang and X. H. Gao, *Int. J. Electrochem. Sci.*, 10(2015)6820.
22. Y. S. Choi, S. Nesic and S. Ling, *Electrochim. Acta*, 56(2011)1752.
23. H. W. Wang, P. Zhou, S. W. Huang and C. Yu, *Int. J. Electrochem. Sci.*, 11(2016)1293.
24. L. Q. Guo, X. M. Zhao, B. C. Wang, Y. Bai and B. Z. Xu, *Corros. Sci.*, 70(2013)188.
25. A. M. Zimer, M. A. S. De Carra, E. C. Rios, E. C. Pereira and L. H. Mascaro, *Corros. Sci.*, 76(2013)27.
26. P. P. Bai, S. Q. Zheng and C. F. Chen, *Mater. Chem. Phys.*, 159(2015)295.
27. M. Liu, J. Q. Wang, W. Ke and E. H. Han, *J. Mater. Sci. Technol.*, 30(2014)504.
28. D. W. Shoosmith, P. Taylor, M. G. Bailey and D. G. Owen, *J. Electrochem. Soc.*, 127(1980)1007.
29. F. X. Shi, L. Zhang, J. W. Yang, M. X. Lu, J. G. Ding and H. Li, *Corros. Sci.*, 102(2016)103.
30. W. F. Li, Y. J. Zhou and Y. Xue, *J. Wuhan. Univ. Technol. Mater. Sci.*, 28(2015)1038.
31. M. N. Iman, *Engineering Failure Analysis*, 2(2014)1.
32. H. W. Wang, C. Yu, S. X. Wang, J. Gao, *Int. J. Electrochem. Sci.*, 10(2015)1169.